JST

http://penerbit.uthm.edu.my/ojs/index.php/jst
ISSN : 2229-8460 e-ISSN : 2600-7924

Journal of Science and Technology

Optimised Photocatalytic Degradation of Crystal Violet Over 1wt% MgO-ZnO Composite Catalyst

Sa'adatu Abdul-aziz Umar[1], Umar Ibrahim Gaya[1*]

[1]Department of Pure and Industrial Chemistry,
Bayero University, Kano, 700241, NIGERIA

*Corresponding Author

DOI: https://doi.org/10.30880/jst.2019.11.01.003
Received 7 May 2019; Accepted 1 June 2019; Available online 17 June 2019

Abstract: Crystal violet is a member of toxic, environmentally ubiquitous basic dyes that must be eliminated. In this paper, the photocatalytic removal efficiency of this dye by a 1wt % MgO-ZnO nanocomposite, synthesized by impregnating ZnO with $Mg(NO_3)_2$ is reported. The catalyst was characterized by x-ray diffraction (XRD), scanning electron microscopy (SEM) and UV-Vis spectrometry. The degradation and mineralization of crystal violet were monitored UV-Visible spectrophotometer and total organic carbon analyzer. The XRD analysis of the catalyst revealed a hexagonal wurtzite structure. The effect of operating variables such as initial crystal violet concentration, catalyst concentration and pH of the solution was optimized using the Box-Behnken design and response surface methodology. The degradation model was statistically remarkable with $p<0.0001\%$. With 10 mg/L initial crystal violet solution, the maximum degradation efficiency of prepared catalyst was found to be 94.6 %. The degradation kinetics agreed with the Langmuir-Hinshelwood model. However, only 60% of total crystal violet-based organic carbon was removed from the solution due to recalcitrance of this environmentally important compound.

Keywords: Photocatalysis, crystal violet, mineralization, ZnO, Box-Behnken

1. Introduction

Dyes are produced and used in very large quantities for various industrial and purposes. Their effluents are considered major water pollutants largely because their degradation products are mostly carcinogenic and toxic for all living organism [1]. Approximately 15% of dyes produced were estimated to be lost during dyeing processes and released into the environment as textile effluent [2]. From synthetic standpoint, dyes can be classified into triphenylmethane, azo or anthraquinone dye groups. Generally, synthetic dyes are recalcitrant in the environment. For instance, the photocatalytic removal of reactive orange 5, an azo dye, in presence of MgO nanopowder recorded 90 % efficiency after 24 h of irradiation [3]. Basic triphenylmethane dyes, having $(C_6H_5)_3CH$ backbone, represent one of the oldest synthetic dyes that are commonly used in textile industry to provide vibrant bright colors to wool, silk, polyamide, food, cosmetics, waxes, paper, leather and plastics. They are brilliant, intense colored, highly colorfast organic dyes. Due to their complex aromatic structures and synthetic origins, these dyes are highly resistant to biodegradation [4]. Two of the well-known triphenylmethane dyes are malachite green and crystal violet. The crystal violet (CV) specifically has found application in antifungal and antimicrobial agent, cosmetic, food, paper, paint, printing and textile industries. Unfortunately, this dye has been classified as a non-biodegradable due to its long half-life in a variety of environments and resistance to biodegradation [5].

Traditional methods used for treatment of dye effluents include physical methods such as adsorption [6] and coagulation [7] can only remove the dye without being transformed into benign substances. Advanced oxidation

*Corresponding author: uigaya.chm@buk.edu.ng

processes are a collection of economically amicable methods which rely on hydroxyl radical for the removal of even the most recalcitrant organic compounds from the environment. In heterogeneous photocatalysis, a semiconductor such as ZnO (with band gap of 3.37 at room temperature) [8, 9], absorbs light of energy greater than or equal to its bandgap to excite electrons from valence band (VB) to conduction band (CB) leaving a hole in the valence band. The hole acts as an oxidant or generator of secondary oxidants such as hydroxyl radicals that can readily degrade organic compounds [10, 11]. However, zinc oxide presents challenges for commercialization which include fast recombination rate, low quantum yield in photocatalytic reactions [12], partial surface dissolution at extreme pH conditions and/or photocorrosion in solution. As a result, the need for modification of this catalyst became imperative. Approaches described in the literature include doping with impurities such as metals, non-metals and oxides. Recently for instance, the degradation of some azo dyes (acid red 27, reactive red 120, tryptopan blue) was found to be more efficient in presence of Bi-doped ZnO than over bare ZnO [13].

The improvement of photocatalytic efficiency of semiconductor catalysts by coupling with oxides has been variously demonstrated. Titania consisting of 5 to 10 wt % ZrO_2 resulted in ~15 to 30 % improvement in photocatalytic efficiency for CV removal [14]. Even though 96 % photocatalytic efficiency for CV degradation and complete mineralization in presence of ZnO has been reported, the analysis of mineralization was based on the disappearance peak of this compound on mass spectrum [15]. While the mineralization of CV can be confirmed by this approach, the degradation products were left unaccounted. In a different study, composite of CeO_2-ZnO showed remarkable photocatalytic performance in the degradation of crystal violet with rate constant of 0.0125 min^{-1} under UV irradiation [16]. We invoke the use of impregnation derived 1 wt% MgO-ZnO composite in this study, for the photocatalytic degradation of crystal violet. This catalyst will be characterized using powder x-ray diffraction analysis and scanning electron microscopy. The degradation of CV will be monitored by UV-Vis spectromentry and the extent of mineralization will be confirmed by total organic carbon analysis. Unlike in the previous CV degradation studies, the effect of operating parameters will be optimized using experimental design based on Box-Behnken method. MgO has a wide band gap in the bulk form (7.8 eV), and unlike CeO_2, it is a non-toxic material. Recently, this oxide has been variously used in highly photoactive nanocomposites such as ZnO-ZnMgO-MgO [17], MgO-$MgFe_2O_4$ [18] and MgO/g-C_3N_4 [19].

2. Materials and Methods

2.1 Chemicals

The crystal violet (98%) and ZnO (99 %; band gap 3.22 eV) were obtained from Sigma-Aldrich while $Mg(NO_3)_2$ (98%) was a British Drug House (BDH) product. The structure of the former is shown in Figure 1. Sodium hydroxide and sulfuric acid were used as pH adjustment chemicals. All solutions were prepared using deionized water. Dye stock solutions were prepared by dissolving 1.02041 g of crystal violet in a liter of deionized water. Desired concentrations were prepared by serial dilution.

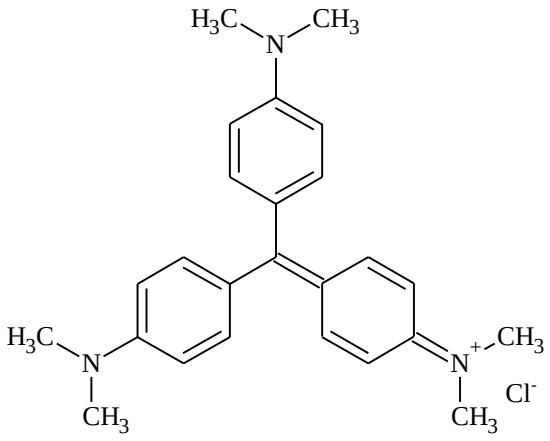

Fig. 1 - Structure of crystal violet.

2.2 Catalyst Synthesis

The catalyst 1wt% of MgO-ZnO was synthesized by a wet impregnation method previously described by [16]. A suspension of 0.99 mol of ZnO in 100 ml of water containing 0.01 mol of $Mg(NO_3)_2$ allowed to stand for 24 h. Water was evaporated in an oven overnight at 110 ºC. The dried solid were ground in an agate mortar and calcined at 400˚C for 6 h in a muffle furnace. The average size of the crystallites and the structure of the as-synthesized catalyst were analyzed using an X'Pert Pro (Philips) diffractometer with Cu-Kα radiation (λ = 0.15406 nm) and a proportional counter as a

detector. The XRD patterns were recorded in the 2θ range of 20°-120° at a scan rate of 4°/min and Cu Kα wavelength of 0.15406 nm. The morphology of the Mg(1 wt%)-ZnO was recorded on a SEM Leica 440 instrument at accelerating voltage of 10 kV and 500x magnification. The band gap energy of this catalyst (3.22 eV) was estimated using Perkin Elmer Lambda 35 UV–Vis spectrometer using the Tauc's relation.

2.3 Photoexperiments

The batch experiments were carried out in a reactor previously described [20], according to a three-level, three-factor Box-Behnken design. The three operating factors were the initial CV concentration (A), catalyst dose (B) and pH (C) varied through three levels as shown in Table 1. Fifteen experiments were performed based on combinations of these input variables under irradiation with a 100 W UV lamp. In each experiment, samples were taken at intervals of 30 min over a period 180 min, and absorbance was measured at 380 nm using Perkin Elmer version lambda 35 UV Vis spectrophotometer. The percent degradation of CV ($\%D_{exp}$) was calculated using Eq. 1 and these were processed using Design Expert version 10 to obtain statistically valid predicted percent degradation values ($\%D_{pred}$).

$$\%D_{\exp} = \frac{[CV]_o - [CV]_t}{[CV]} \text{ x } 100 \qquad (1)$$

Where $[CV]_o$ (mg/L) is initial dye concentration of the crystal violet and $[CV]_t$ (mg/L) is concentration of the crystal violet at irradiation time t (min).

Table 1 - Input factors and levels used in the study.

Factors	Levels (and codes)		
A-CV concentration (mg/L)	10 (-1)	20(0)	30(+1)
B- 1wt% of MgO-ZnO (g/L)	0.1(-1)	0.3(0)	0.5(+1)
C-pH	3(-1)	8(0)	11(+1)

3. Results and Discussion

3.1 Catalyst Characterization

The XRD patterns of as-synthesized 1 wt% MgO doped ZnO nano-particles are shown in Fig. 2. The XRD patterns shows peaks at the diffraction angles (and reflections) of = 32.8 (100), 34.64 (002), 36.5 (101), 47.47 (102), 56.76 (110), 63.08 (103), 68.01 (200) and 68.29 (112) corresponding to hexagonal wurtzite ZnO (JCPD card 36-1451) [21, 22]. The diffraction angle 42.88° is characteristic of MgO (JCPDS file 01-072-0447). By using Debye-Scherer equation, the average particle size of the composite was calculated to be 34 nm. The extreme sharpness of the diffraction peaks in Fig. 2 are evidences of the high crystallinity of the nanocomposite particles.

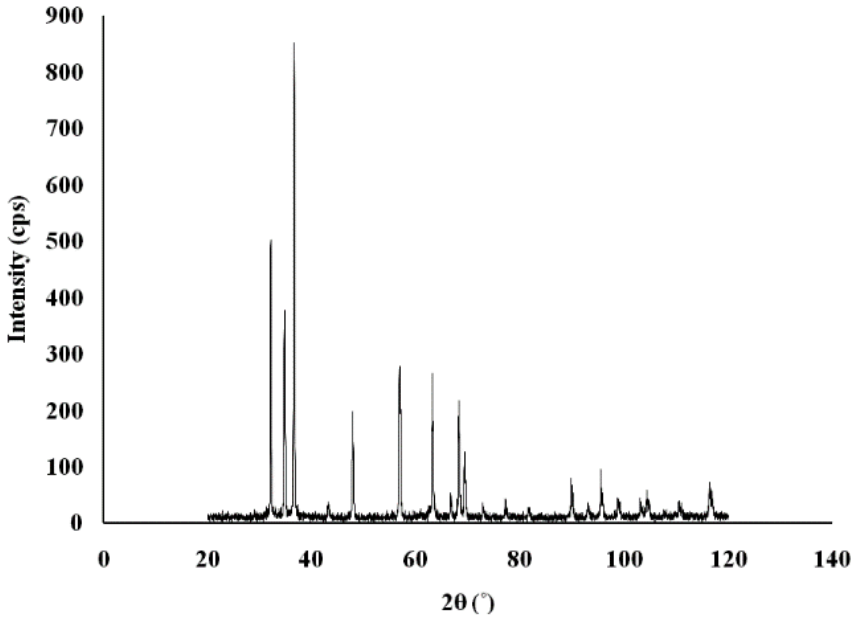

Fig. 2 -The XRD patterns of the synthesized 1wt%MgO doped ZnO catalyst.

The surface morphology of the ZnO and MgO doped ZnO catalyst was examined using scanning electron microscope with and without MgO, at accelerating voltage of 10 kV and scale of 200μm (Fig. 3 a and b). Both SEM images show agglomerates of bulk micrometer grain particulates without clear distinction of the effect of the 1wt% MgO augmented.

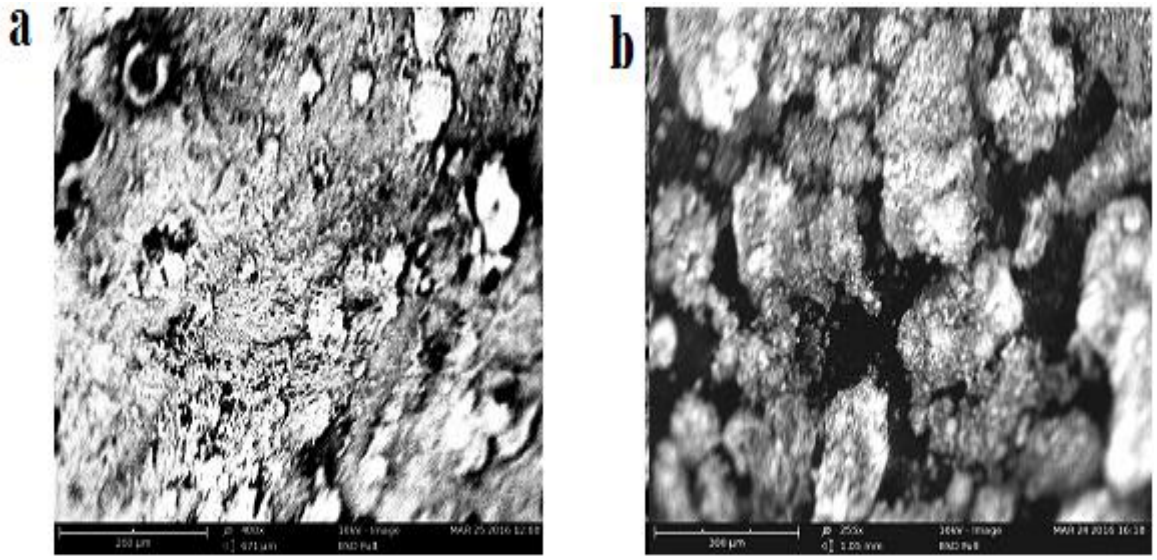

Fig. 3.-The SEM image of (a) bare ZnO (b) 1wt % MgO-ZnO.

3.2 Box-Behnken Experimental Design

The efficiencies of the various photoexperiments (% D_{exp}) and those statistically predicted (% D_{pred}) conducted based on the Box-Behnken design are shown in Table 2. Parameters in the Table are shown in both their actual and coded levels. As seen from the table, there is great consistence between the experimental and the predicted degradation efficiencies. This is confirmed by the plot of predicted versus actual degradation efficiencies which shows a remarkable fit with almost all the points lying on a straight line. The optimum conditions of the study were 10 mg/L initial crystal violet concentration, 0.1 g/L catalyst concentration and pH 8, in which 94.6% degradation was achieved.

Table 2 - The Box-Behnken efficiencies for photocatalytic degradation of crystal violet.

S/No.	A: [CV] (mg/L)	B: 1wt% of MgO-ZnO (g/L)	C: pH	D_{exp}(%)	D_{pred}(%)
1	20(0.00)	0.5(1.00)	3(-1.00)	88.0	87.74
2	20(0.00)	0.3(0.00)	8(0.00)	92.8	92.56
3	30(1.00)	0.3(0.00)	3(-1.00)	81.9	82.02
4	30(1.00)	0.5(1.00)	8(0.00)	85.0	85.44
5	20(0.00)	0.1(-1.00)	3(-1.00)	89.0	89.14
6	20(0.00)	0.5(1.00)	11(1.00)	90.0	90.02
7	30(1.00)	0.3(0.00)	11(1.00)	84.7	84.30
8	20(0.00)	0.3(0.00)	8(0.00)	91.9	92.56
9	30(1.00)	0.1(-1.00)	8(0.00)	87.0	86.82
10	10(-1.00)	0.3(0.00)	3(-1.00)	89.7	89.70
11	20(0.00)	0.3(0.00)	8(0.00)	92.8	92.56
12	20(0.00)	0.1(-1.00)	11(1.00)	91.0	91.42
13	10(-1.00)	0.5(1.00)	8(0.00)	93.0	93.12
14	20(0.00)	0.3(0.00)	8(0.00)	92.8	92.56
15	10(-1.00)	0.3(0.00)	11(1.00)	92.0	91.97
16	20(0.00)	0.00	8(0.00)	92.8	92.56
17	10(-1.00)	-1.00	8(0.00)	94.6	94.52

The predicted relationship between the degradation efficiency of crystal violet (% D) under the influence of initial crystal violet concentration (A), catalyst concentration (B) and pH (C) is described by the quadratic model described by Eq. 2. From the equation, the cross terms do not influence the crystal violet degradation.

$$\%D_{pred} = 92.56 - 3.84A - 0.70B + 1.14C - 2.58A^2 - 2.98C^2 \quad (2)$$

The adequacy of this model can adjudged by the analysis of variance (ANOVA) in Table 3. From the table, the model is remarkably significant with $p<0.0001$, an insignificant lack of fit (LOF = 0.61), and F-value of 329.71 (a 0.01% chance of the value being due to noise). All the model terms (A, B, C, A^2, C^2) are significant. The analysis also showed a reasonable agreement of the Pred R-Squared value (0.9849) with the Adj R-Squared value (0.9904).

Table 3 - ANOVA for Response Surface Quadratic Model

Source	Sum of Squares	Degree of freedom	Mean square	F-value	Prob > F	Remark
Model	201.52	5	40.30	329.71	< 0.0001	Significant
A	117.81	1	117.81	963.71	< 0.0001	
B	3.92	1	3.92	32.07	0.0001	
C	10.35	1	10.35	84.68	< 0.0001	
A^2	28.11	1	28011	229.97	< 0.0001	
C^2	37.50	1	37.50	306.79	< 0.0001	
Residual	1.34	11	0.12			
Lack of Fit	0.70	7	0.100	0.61	0.7311	not significant
Pure Error	0.65	4	0.16			
Cor Total	202.86	16				

The response surface plots showing effect of parameters are shown in Fig. 4. Figure 4a shows low degradation efficiencies at high initial crystal violet concentration and pH. Accordingly, the 3D plot of catalyst doses vis-à-vis crystal violet concentration (Fig. 4b) shows high degradation efficiencies only as these parameters are lowered.

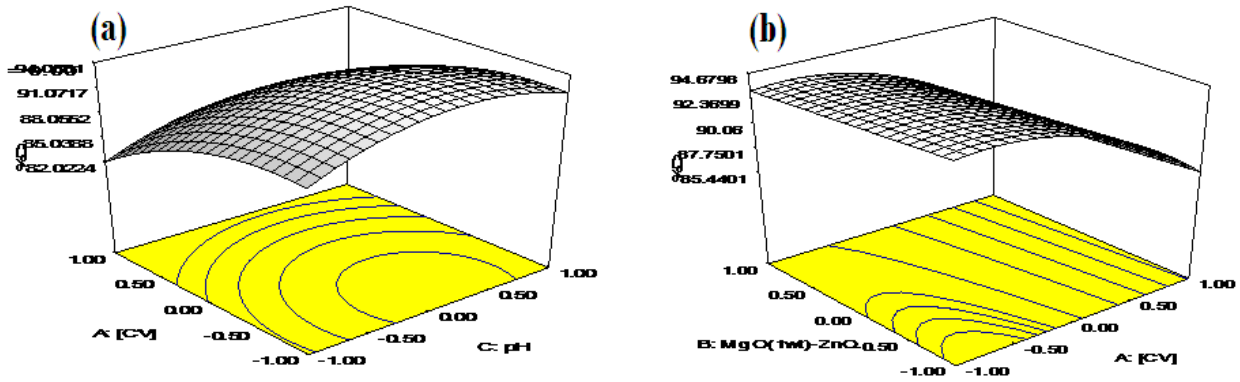

Fig. 4 - Response plots showing the interaction of crystal violet concentration with (a) pH, (b) catalyst.

3.3 Mineralization

Customarily, mineralization is measured using total organic carbon (TOC) analyzer. In this study, the mineralization was monitored at 20 mg/L initial crystal violet concentration, 0.3 g/L catalyst concentration and pH 8, which corresponds to the experiments at the center point of our Box-behnken design. The results obtained (Fig. 5) show continuous decrease in % TOC with irradiation which in turn equivalently implies mineralization of the crystal violet. It would be seen from

the Fig. 5 that the TOC is steadily decreased with increasing irradiation, which indicates the disappearance of crystal violet, the result showed that 60% is removed from the crystal violet solution. The incomplete mineralization of crystal violet shows that degradation proceeds at a faster rate than mineralization, indicating the imperative for checking the level of mineralization.

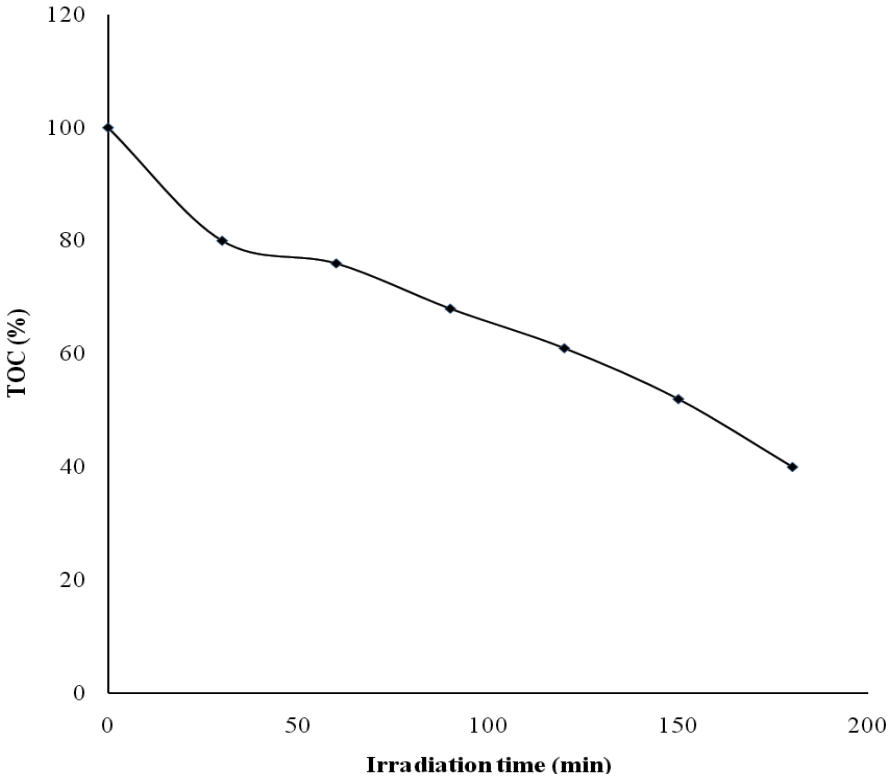

Fig. 5 - Variation of TOC removal with irradiation time.

3.4 Kinetics of Crystal Violet Degradation

The Langmuir-Hinshelwood rate expression has been used to describe the relationship between the heterogeneous photocatalytic degradation rate and the initial pollutant concentration. Basically, the rate of removal of CV may be given by equation (Eq. 3).

$$r = -\frac{d[\mathrm{CV}]}{dt} = \frac{k_r k_e [\mathrm{CV}]}{1 + k_e [\mathrm{CV}]} \tag{3}$$

Where k_r is the reaction rate constant (mg/L.min) and k_e is the adsorption coefficient of the CV onto the photocatalyst particle (L/mg). At low CV concentration, the rate of photo-reaction can be simplified to an apparent first-order equation (Eq. 4),

$$-\frac{d[\mathrm{CV}]}{dt} = k_r k_e [\mathrm{CV}] \tag{4}$$

Let $k_{app}=k_r k_e$, so that Eq. 4 yields the differential rate of CV degradation (Eq. 5).

$$-\frac{d[\mathrm{CV}]}{dt} = k_{app} [\mathrm{CV}] \tag{5}$$

Where the k_{app} is the apparent pseudo-first-order constant Eq. 6 is an integrated version of Eq. 5.

$$\ln \frac{\mathrm{C_o}}{\mathrm{C_t}} = k_{app} \mathrm{t} \tag{6}$$

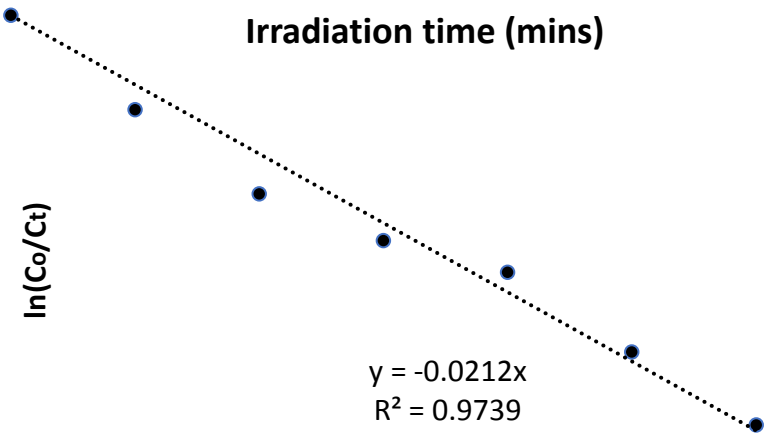

Fig. 6 - Langmuir-Hinshelwood plot of CV degradation in 1wt%MgO-ZnO.

In this study, experimental results at optimum conditions (Fig. 6) indicated a reasonable agreement of the photodegradation rate of CV in presence of UV/1%MgO-ZnO (R^2 = 0.973) with the linear form of the Langmuir-Hinshelwood (L-H) kinetics. The k_{app} realized (0.021 min^{-1}) is much higher than that of the photocatalytic degradation of reactive red 4 over TiO_2 immobilized on glass (0.002 min^{-1}) but less than the performance of TiO_2/chitosan layer immobilized on glass (0.064 min^{-1}) [23] due to the outstanding synergistic effect of the combined photocatalysis-adsorption process delivered by this layer.

3.5 Recyclability of 1wt% MgO-Doped ZnO

Catalyst reusability can make the catalyst more attractive for full-scale application. The reusability of the 1wt% MgO doped ZnO at optimized conditions obtained from the Box-behnken design (10 mg/L crystal violet, 0.1 g/L catalyst and pH 8). After each run, the photocatalyst was recovered, washed with deionized water to remove the adsorbed crystal violet dye molecules. The photocatalyst was reactivated by calcination at 300 ^oC in furnace for 2 h for next photocatalytic reaction. The results showed in Fig. 7 that the fresh catalyst (with 97 % removal efficiency) can be reused for four consecutive runs with at least 94% removal. At the fifth cycle, the % CV removal was only 88% possibly due to fouling [24] or photocorrosion with long time irradiation [25]. Nonetheless, the least performance obtained in this stability study is similar and in some cycles better than that of TiO_2 in presence of methyl orange dye solutions [26].

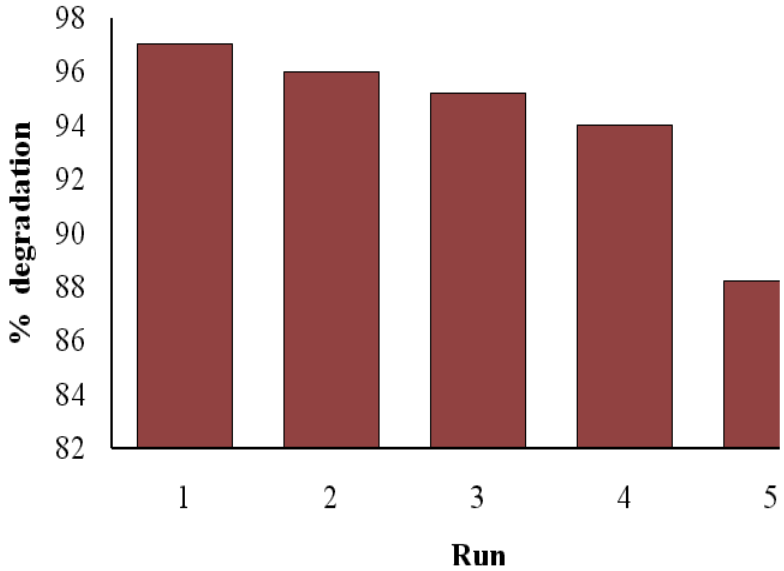

Fig. 7 - Plot showing reusability of 1% MgO doped ZnO in crystal violet degradation.

4. Conclusion

Photocatalytic degradation of crystal violet was carried out by 1wt % MgO doped ZnO under UV irradiation. The synthesized catalyst was characterized using XRD, SEM and UV-Visible spectrometry. Analysis of the XRD confirmed the presence of MgO and hexagonal Wurtzite ZnO structure. The variables such as the amount of photocatalyst, crystal violet concentration and pH were successfully studied. The maximum degradation was achieved at pH of 11, 10 mg/L of the crystal violet concentration and 0.1g/l of catalyst. A reusability study shows that 1% MgO doped ZnO can be reused at least 4 times. Even though degradation at the Box-Behnken center points was nearly complete (92.8 %), accomplishment of mineralization under the same conditions was far from being achieved (60 %) which implies the existence of recalcitrant degradation products in solution.

Acknowledgement

Sa'adatu Umar is grateful to Hamza Rabiu Sani and Abubakar Hamisu for constructive criticisms during her days as M.Sc. student and for assistance with XRD calculations, respectively.

References

[1] Raja, V.R., Rosaline, D.R., Suganthi, A., & Rajarajan, M. (2018). Facile sonochemical synthesis of Zn_2SnO_4-V_2O_5 nanocomposite as an effective photocatalyst for degradation of Eosin yellow. Ultrasonics Sonochemistry, 44, 310-318.

[2] Bessekhouard, Y., Robert, D., & Weber, J.V. (2004). Bi_2S_3/TiO_2 and CdS/TiO_2 heterojunctions as an available configuration for photocatalytically degradation of organic pollutant, J. Photochemistry and Photobiology. A, 163, 569-580.

[3] Kamel, M.M., Mashaly, H.M., & Abdelghaffar, F. (2013). Photocatalyst Decolorization of Reactive orange 5 dye using MgO nano powder and H_2O_2 Solution. *World Applied Sciences Journal*, 26, 1053-1060.

[4] Godlewska, E.Z., Przystas, W., & Sota, E.G. (2014). Decolorization of different dyes by two Pseudomonas strains under various growth conditions. Water Air Soil Pollution, 225, 1-13.

[5] Rehman, F., Sayed, M., Khan, J.A., Shah, L.A., Shah, N.S., Khan, H.M., et al. (2018). Degradation of crystal violet dye by Fenton and photo-Fenton oxidation processes. Zeitschrift für Physikalische Chemie, 232, 1-16.

[6] Sarma, G.K., Gupta, S.S., Bhattacharyya, K.G. (2016). Adsorption of crystal violet on raw and acid-treated montmorillonite, K10, in aqueous suspension. Journal of Environmental Management, 171, 1-10.

[7] Vijay, E.V.V., Jerold, M., Ramya, M.S., Lakshmanan, S., & Sivasubramanian, V. (2018). Electrocoagulation using commercial grade aluminium electrode for the removal of crystal violet from aqueous solution. Water Science and Technology, 79, 597-606.

[8] Fan, J.C., Sreekanth, K.M., Xie, Z., Chang, S.L., Rao, K.V. (2013). p-Type ZnO materials: Theory, growth, properties and devices. Progress in Materials Science, 58, 874-985.

[9] Das, J., & Kushalani, D. (2010). Nonhydrolytic Route for Synthesis of ZnO and Its Use as a Recyclable Photocatalyst . Journal of Physical Chemistry C, 114, 2544-2550.

[10] Oppong, S.O.-B., Anku, W.W., Opoku, F., Shukla, S.K., & Govender, P.P. (2018). Photodegradation of

eosin yellow dye in water under simulated solar light irradiation using La–doped ZnO nanostructure decorated on graphene oxide as an advanced photocatalyst. ChemistrySelect, 3, 1180– 1188.

[11] Wang, C., Tan, C., Lv, W., Zhu, G., Wei, Z., Zhang, K.H.L., et al. (2018). Coherent Bi_2O_3-TiO_2 hetero-junction material through oriented growth as an efficient photo-catalyst for methyl orange degradation. Materials Today Chemistry, 8, 36-41.

[12] Zhu, Y.-P., Li, M.,Liu, Y.-L., Ren, T.-Z., & Yuan, Z.-Y. (2014). Carbon-doped ZnO hybridized homogeneously with graphitic carbon nitride nanocomposites for photocatalysis. Journal of Physical Chemistry C, 114, 10963-10971.

[13] Sasikala R., & Subash, B. (2019). Synthesis, characterization of Bi/ZnO and its photoactivity towards TB, AR 27 & RR 120 degradation under UV-A light. Optik, 178, 1079-1089.

[14] Marija, B.V., Marjan, S.R., Milan, Z.M., Branko, Z.M., & Aleksandra, R.Z. (2016). Degradation of crystal violet over heterogeneous TiO_2-based catalysts: the effect of process parameters. Processing and Application of Ceramics, 10,189–198.

[15] Ameen, S., Akhtar, M.S., Nazim, M., Shin, H.S., (2013). Rapid photocatalytic degradation of crystal violet dye over ZnO flower nanomaterials, Materials Letters 96 (2013) 228–232.

[16] Zahoor, M., Arshad, A., Khan, Y., Iqbal, M., Bajwa, S.Z., Soomro, R.A., et al. (2018). Enhanced photocatalytic performance of CeO_2–TiO_2 nanocomposite for degradation of crystal violet dye and industrial waste effluent. Applied Nanoscience, 8, 1091-1099.

[17] Abed, C., Ali, M.B., Addad, A., & Elhouichet, H. (2019). Growth, structural and optical properties of ZnO-ZnMgO-MgO nanocomposites and their photocatalytic activity under sunlight irradiation. Materials Research Bulletin, 110, 230-238.

[18] Ramos-Ramírez, E., Tzompantzi-Morales, F., Gutiérrez-Ortega, N., Mojica-Calvillo, H.G., & Castillo-Rodríguez, J. (2019). Photocatalytic Degradation of 2,4,6-Trichlorophenol by MgO–$MgFe_2O_4$ Derived from Layered Double Hydroxide Structures

[19] Mao, N., & Jiang, J.-X. (2019). MgO/g-C_3N_4 nanocomposites as efficient water splitting photocatalysts under visible light irradiation. Applied Surface Science, 476, 144-150.

[20] Yusuf, A., Gaya, U. (2018). Mechanochemical synthesis and characterization of N-doped TiO_2 for photocatalytic degradation of caffeine. Nanochemistry Research, 3, 29-35.

[21] Zheng, Y., Zheng, L., Zhan, Y., Lin, X., Zheng, Q., & Wei, K. (2007). Ag/ZnO Heterostructure nanocrystals: synthesis, characterization, and photocatalysis. Inorganic Chemistry, 46, 6980-6986.

[22] Yu, J., & Yu, X. (2008). Hydrothermal synthesis and photocatalytic activity of zinc oxide hollow spheres. Environmental Science and Technology, 42, 4902-4907.

[23] Nawi, M.A., & Sheilatina, S.S. (2012). Photocatalytic decolourisation of Reactive Red 4 dye by an immobilised TiO_2/chitosan layer by layer system. Journal of Colloid and Interface Science, 372, 80–87.

[24] Chakrabarti, S., & Dutta, B.K. (2004). Photocatalytic degradation of model textile dyes in wastewater using ZnO as semiconductor catalyst. Journal of Hazardous Materials B, 112, 269–278.

[25] Zhang, H., Chen, G., & Bahnemann, D.W. (2009). Photoelectrocatalytic materials for environmental applications. Journal of Materials Chemistry, 19, 5089–5121.

[26] Carcel, R.A., Andronic, L., & Duta, A. (2012). Photocatalytic activity and stability of TiO_2 and WO_3 thin films. Materials Characterization, 40, 68-73.